Aeroelastic tailoring for static and dynamic loads with blending constraints

Bordogna, Marco Tito; Lancelot, Paul; Bettebghor, Dimitri; De Breuker, Roeland

Publication date
2017

Document Version
Accepted author manuscript

Published in
17th International Forum on Aeroelasticity and Structural Dynamics, IFASD 2017

Aeroelastic Tailoring for Static and Dynamic Loads with Blending Constraints

Marco Tito Bordogna[1,2], Paul Lancelot[2], Dimitri Bettebghor[1] and Roeland De Breuker[2]

[1] *ONERA, The French Aerospace Lab, F-92322 Châtillon, France*
[2] *Faculty of Aerospace Engineering, Delft University of Technology, 2629 HS Delft, The Netherlands*

Abstract

In the present paper the authors want to investigate the effect of different load configuration in order to identify the ones driving the optimization. A set of static loads, gust loads and static loads with maneuver load alleviation (MLA) are tested. Gust loads have been included in the optimization via an equivalent static load (ESL). Composite blending is tackled by means of continuous constraints and a two phases approach is proposed to find a blended stacking sequence table. Results show that region of influence can be identified for specific loads and that MLA can be beneficial for structural weight reduction. Finally, the blending constraints prove their effectiveness by significantly reducing the error in retrieving a blended stacking sequence.

Keywords: Aeroelastic Tailoring, Gust, ESL, Blending, Composite

The work included in this paper has originally been presented during the *International Forum on Aeroelasticity and Structural Dynamics (IFASD, 25-28 June 2017, Como - Italy)*. The present paper is an updated version of the conference proceeding. The updates concern mainly the results and conclusions sections.

1 Introduction

Aeroelastic tailoring is a field of research which has received increased attention over the past decades since its very first definition by Shirk et al. [1] in the late 90's . This is thanks to the development of light-weight and highly flexible wings for modern airliners and long endurance aircraft. It has been identified as an efficient way to improve aerodynamic performance while reducing loads and therefore structural weight [2]. Using variable stiffness laminates, the wing structure can be tailored in such way that it will relieve itself from the loads during maneuvers and gusts, while maintaining an optimal aerodynamic shape in cruise. Nonetheless, constraints related to structural strength and stiffness, aeroelastic instability and minimum control effectiveness in flight still apply. All civil aircraft must comply with the certification specifications, and yet be as light as possible. The conventional structural sizing process is mostly driven by fixed loads and by aeroelastic instability constraints [3]. Taking dynamic aeroelastic load cases earlier in the design process could be beneficial in term of performance and could reduce the non-feasibility of the design, Kenway et al. [4] shows that a wing optimized for fixed loads can fail when subjected to discrete gust. Moreover, these dynamic loads are

also influenced by the rigid body motion of the aircraft as shown by Reimer et al. [5] and therefore more difficult to predict.

The use of composite materials to build large structures remains also one of the main challenges of today's aircraft industry. Despite offering improved mechanical performances with higher strength to weight ratio as compared to their conventional aluminium counterparts, composites are more difficult to design because of the increased number of design variables due to the anisotropy of the material and the many manufacturing constraints. Ply angles need to be correctly chosen to determine the optimal stiffness of the laminate in order to minimize or maximize a certain behavior or characteristic of the laminate. Finally, for large composite structure, local section optimization can lead significant thickness and/or stacking sequence variations between adjacent sections. As a consequence, not considering ply continuity (i.e. blending) early in the design phase will reduce structural integrity at sections intersection or could results in hardly manufacturable solutions [6, 7].

Two reference works on static aeroelastic tailoring with local panel optimization are the ones from B. Liu [8] and J. Dillinger [6]. Even though the two works focus on the same topic, they do not use the same problem decomposition approach and they considered blending differently. Liu used a Quasi separable Subsystem Decomposition (QSD) leading to a sequential optimization where the author introduced two blending constraints, one at each step. J. Dillinger used an AIO (*All-in-one*) approach, where a gradient-based (continuous) optimization of homogenized stiffness parameters (e.g. lamination parameters) is performed to obtain the optimum solution. Later a genetic algorithm (discrete optimization) is used to retrieve feasible stacking sequences while enforcing blending.

Several authors have used bi-step strategies, however, due to the difficulties in enforcing discrete blending constraints in the gradient-based optimization, different sets of constraints are used in the two subsequent optimization steps resulting in significant discrepancies between the two solutions. This does no guarantee to find an equivalent of the optimal continuous design in the discrete domain. Recently, Macquart et al. [9] proposed employing lamination parameters combined with a set of blending constraints to be used in the continuous optimization in order to achieve more realistic and manufacturable continuous designs. In [9] the continuous blending constraints have been applied to the benchmark case of the 18 panel horseshoe to prove the effectiveness of the blending method. In a continuing effort, the authors [10] have also demonstrated that the application of blending constraints during aeroelastic optimizations with strain and buckling constraints results in more realistic continuous designs.

In the first part of the paper the authors focus on the identification of the critical loads in aeroelastic tailoring. Static load cases are employed together with gust responses to identify which load configuration is more critical. The effect of performing maneuver load alleviation (MLA) during 2.5g and -1g over the identification of the critical load is assessed. In the second part, an approach to ensure the satisfaction of blending requirements is presented and the effect of the blending over the critical loads is evaluated.

The paper is divided as following. In Sec. 2 the concept of blending is introduced together with the composite parametrization chosen. Then, in Sec. 3 the optimization strategies used in the paper are explained together with the concept of equivalent static load (ESL). The test case used in this work in introduce in Sec. 4 and finally the results are presented and commented in Sec. 5.

2 Blending

The use of composite materials to build large structures remains one of the main challenges of today's aircraft industry. Despite offering improved mechanical performances with higher strength to weight ratio as compared to their conventional aluminium counterparts, they are more difficult to design because of the increased number of design variables due to the anisotropy of the material and the many manufacturing constraints. Moreover, in order to obtain better performing structures, large components are usually divide in sections each of them locally optimize with respect to thickness and composite anisotropy. As consequence the optimization process could results in optimal solution that lack of structural integrity because of significant thickness and/or stacking sequence variations between adjacent sections. Therefore, constraints over ply continuity (i.e. blending) should be taken into account early in the design phase in order to obtain ready-to-manufacture solutions[6, 7].

Several definition of blending have been proposed (Figure 1). Inner and outer blending have been introduced by Adams et al. [11] , in these definitions only the innermost and the outermost plies can be dropped. Two alternative definitions, the generalized and relaxed generalized blending, have been formulated by Van Campen et al. [12]. Generalized blending requires all plies of the thinnest section to be continuous in the whole structure; relaxed generalized blending demands that no discontinuous plies should be in direct physical contact with each other. Throughout this paper, blending is always associated to the generalized blending definition of Van Campen et al. [12] for sake of clarity.

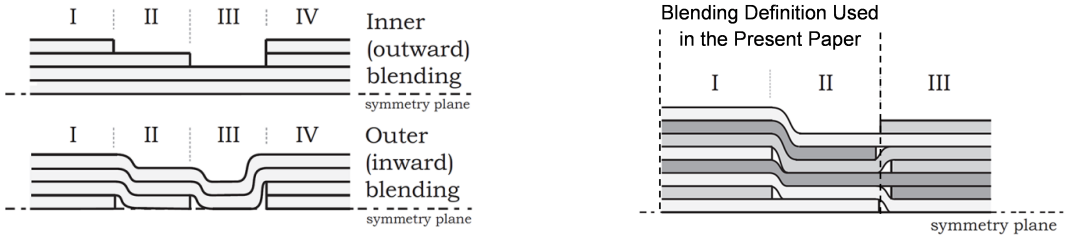

Figure 1: Outward and inward blending on the left, and generalized (I and II) and relaxed generalized (II and III) blending on the right. Original figures from [12] .

In this work, blending among adjacent sections is enforced by means of the continuous blending constraints introduced by Macquart et al. [9] in the lamination parameter space. Lamination parameters (LPs) have been first introduced by Tsai et al.[13] and are used to describe the stiffness matrix of composite laminates in a continuous space. For stacking sequence with discrete plies of constant thickness (t_{ply}) and ply angle (θ_i), lamination parameters are defined in Eqs. 1. In this paper only symmetric stacking sequence with even number of ply and same thickness are considered, therefore only lamination parameters for membrane (A) and bending (D) stiffness matrices are taken into account.

$$
\begin{aligned}
(V_1^A, V_2^A, V_3^A, V_4^A) &= \frac{1}{N}\sum_{i=1}^{N}(\cos 2\theta, \sin 2\theta, \cos 4\theta, \sin 4\theta)\mathrm{dz} \\
(V_1^D, V_2^D, V_3^D, V_4^D) &= \frac{4}{N^3}\sum_{i=1}^{N} z_i^2(\cos 2\theta, \sin 2\theta, \cos 4\theta, \sin 4\theta)\mathrm{dz}
\end{aligned}
\tag{1}
$$

where $z_i = -N/2 + i$

Lamination parameters (LPs) have the advantages of describing the stiffness matrix in a continuos and they define a convex space [14] suitable for gradient-based optimizers. Moreover, any generic stacking sequence can be reproduced with twelve continuous variable plus laminate thickness. On the other hand the use of LPs requires an additional optimization step (usually performed by evolutionary algorithms) that retrieves a discrete stacking sequence from the continuous optimum. Therefore a two phase optimization strategy is required (see Sec. 3).

The key concept for the derivation of the continuous blending constraints is to evaluate the change in lamination parameters (ΔV) due to ply drops. A comprehensive derivation of all the blending constraints can be found in [9]. Here for safe of completeness, the derivation of the blending constraints for a single in-plane lamination parameter (Eq. (6)) is presented.

Lets denote $V^A_{1(N)}$ and $V^A_{1(N-X)}$ the value of the first in-plane lamination parameter when the laminate has respectively N and $N-X$ plies. The change in lamination parameter due to a X ply drops is denoted as $\Delta V^A_{1(N)\rightarrow(N-X)}$ and it is presented in Eq. (4).

$$V^A_{1(N)} = \frac{1}{N}\sum_{i=1}^{N}\cos(2\theta_i) \tag{2}$$

$$V^A_{1(N-X)} = \frac{1}{N-X}\sum_{i=X+1}^{N}\cos(2\theta_i) \tag{3}$$

$$\Delta V^A_{1(N)\rightarrow(N-X)} = V^A_{1(N)} - V^A_{1(N-X)} = \underbrace{\frac{1}{N}\sum_{j=1}^{X}\cos(2\theta_j)}_{\substack{\text{Term containing the}\\ \text{dropped plies}}} + \underbrace{\left(\frac{1}{N}-\frac{1}{N-X}\right)\sum_{i=1}^{N-X}\cos(2\theta_i)}_{\substack{\text{Term containing the plies}\\ \text{present in both sections}}} \tag{4}$$

where X is the number of dropped plies, N is the total number of plies, θ_j represent the orientation of the dropped plies and θ_i the orientation of the plies left in the stacking sequence. The maximum and minimum value of Eq. (4) occurs respectively for $[\theta_j,\theta_i] = [0°,90°]$ and for $[\theta_j,\theta_i] = [90°,0°]$ at which $\Delta V^A_{1(N)\rightarrow(N-X)}$ is:

$$\max_{(\theta_j,\theta_i)} ||\Delta V^A_{1(N)\rightarrow(N-X)}|| = 2\frac{X}{N} \tag{5}$$

This implies that no blendable solution can be found if, in two adjacent sections, the change in V^A_1 is greater than $2(X/N)$. By applying the same approach to the remaining in-plane lamination parameters, it can be shown that this limit holds. Thus, it is possible to define a blending constraint for single in-plane lamination parameter change as:

$$||\Delta V^A_{k(N)\rightarrow(N-X)}|| \leq 2\frac{X}{N}, \qquad \text{for } k = 1,2,3,4 \tag{6}$$

For sake of brevity, the extension of the blending constraints to the higher dimension (i.e. taking into account more LPs) is not covered and the interested reader is invited to check the work of Macquart et al. [9]. However, in order to provide the reader with a visual representation of the constraints, an example of the effect of a 2D blending constraints considering V^A_1 and V^A_2 is herby provided. Lets take into account the situation presented in Figure 2, where a multi-section laminate is subjected to X ply drops from a section with N plies to another with $N-X$ plies. Lets now reproduce this situation in the lamination parameters space for V^A_1 and V^A_2 (Figure 3). In this example the starting laminate section has N equal to 20 plies and it is used to generate all possible $N-X$ plies blended sections by removing

X equal to 2 and 4 plies. Blending constraints for the two different ply drops are shown to be capable of including all possible $N-X$ plies blended sections. A shrinking factor α is added to the constraints to reduce the hypersphere created by the blending equations and therefore tighten the constraints

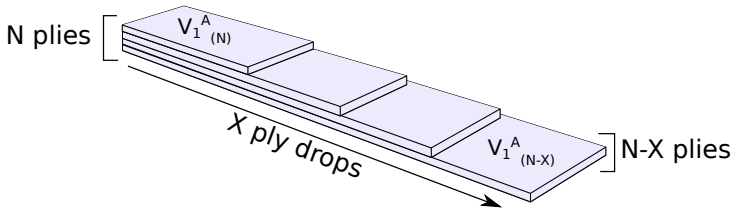

Figure 2: Multi-section laminate and ply-drops illustration

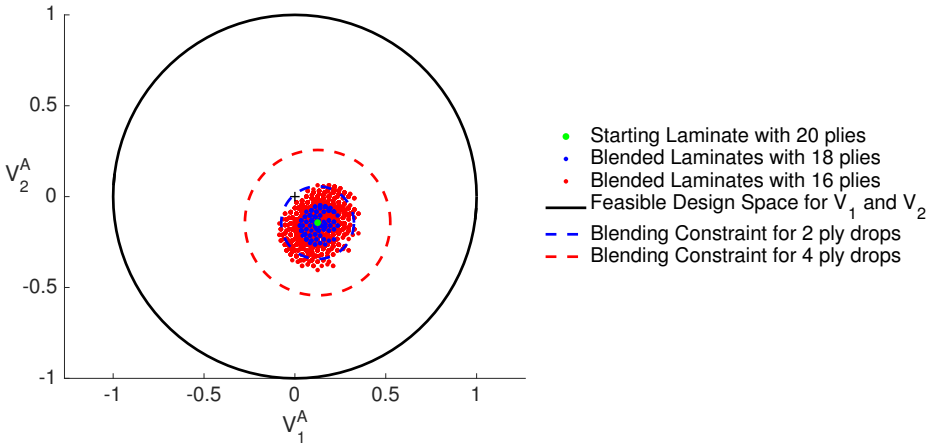

Figure 3: Example of a 20 plies laminate and all its possible blended laminates with 2 and 4 ply drops.

3 Optimization strategy

In this section the optimization strategy is explained. As already mentioned in Sec. 2, the use of lamination parameters require a two-phases approach where a continuous gradiend-based optimization is followed by an inverse optimization problem where, from the optimum LPs, the corresponding stacking sequence is retrieved. The full two-phases optimization is introduced in Sec. 3.2 while in Sec. 3.1 the concept of the equivalent static load (ESL), fundamental to consider the gust case in the optimization, is presented and its implementation explained.

3.1 Equivalent Static Load (ESL)

To perform this optimization, a gradient-based approach is preferred as the number of design variables is relatively large (≈ 400). One issue when accounting for gust loads remains that these loads are highly dependent on the design itself. They are constantly changing during the optimization, as the design evolves with it. However the computation of required sensitivity over a transient response is not an

easy task and can require a lot of function evaluations [15]. Therefore, transient responses are costly to implement into current design optimization process. The equivalent static loads (ESL) method formalized by Kang et al. [16] is used to bypass this issue and provides optimized results for static and dynamics load cases.

In the present work ESL is used with little improvement regarding the original idea as described in Figure 4. Nonetheless, it is worth mentioning that examples of improved ESL method exist in the literature. For instance, Bettebghor et al. [17] proposed to estimate the load sensitivities with surrogate modeling. This work was applied to engine pylon sizing in the event of a "fan blade off", a highly dynamic load case. ESL was extended to different scenarios, most of them summarized by Park [18]. These include non-linear geometries, multi body dynamics, and crash and topology optimization for the automotive industry.

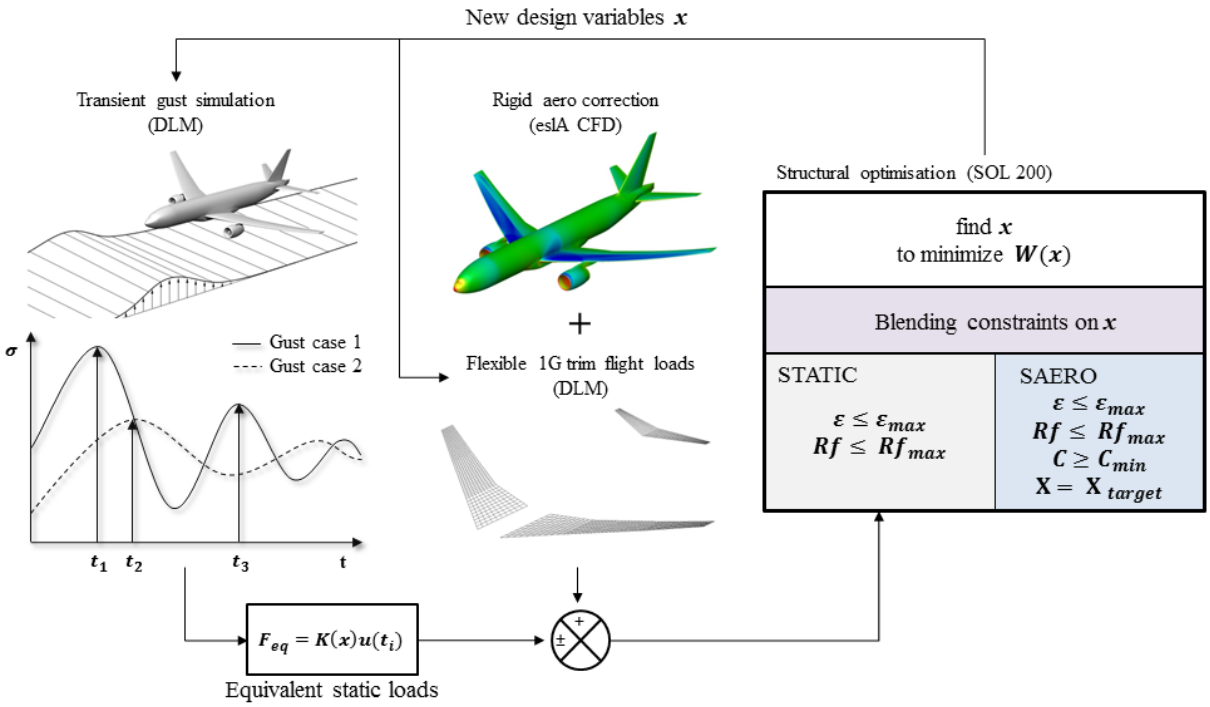

Figure 4: Overview of the equivalent static load process. ELS is incorporated in step 1 and 2 of the optimization process (Sec.3.2).

ESL relies on a weak coupling between the transient simulations and the optimizer. Therefore, it requires several iterations where loads are updated along the new design before a converged solution emerges. The lack of sensitivities between the design variables and the transient responses constitutes one of the main drawback of this method. Therefore, design changes between two consecutive ESL loop need to be small enough to ease constraints satisfactions. Still, this method offers an easy implementation regardless of the different tools used in the loop and can take advantage of already existing gradient based optimization and aeroelastic analysis code. The governing equation that needs to be solved for a gust analysis is the following:

$$M(x)\ddot{u}(t) + K(x)u(t) = f_{\text{gust}}(v_\infty, v_{\text{gust}}(t), \ddot{u}(t), u(t)) \tag{7}$$

where u is the nodal displacement vector, M and K respectively the mass and linear stiffness matrices which are dependent upon the design variables x and f_{gust} the aerodynamic forces due to a gust. Finally, v_{gust} is the vertical speed component of a transient gust and v_∞ the flow speed in the far field. No structural damping is required as the damping forces are provided by the aerodynamic part. Once the displacements computed from the Eq. 7, a set of equivalent static loads f_{eq} can be retrieved from the time steps identified in the elements strain history as the most critical:

$$f_{\text{eq}} = K(x)\,u(t_i) \tag{8}$$

In the case of a free flying aircraft simulation, the structural displacements are obtained by removing the rigid body translations and rotations from the displacement vector of each grid points. The loads are computed at each iteration with the transient aeroelastic module of MSC.Nastran, designated as the Solution 146. This solution relies on the Doublet Lattice Method (DLM) to solve the gust analysis problem. Although Eq. 7 is given as time dependent, MSC.Nastran solves everything in the frequency domain before converting the output results (displacement, strains etc.) in the time domain. This method is limited to linear aerodynamic and structural computation only. Once the set of ESL generated, they are sent to the optimizer module of MSC.Nastran (SOL200) to be treated as a static structural optimization problem. SOL200 can also compute steady aeroelastic loads for which the optimizer has access to the sensitivities and efficiently perform gradient based optimization. In this example the constraints are applied on strength (ϵ), on the buckling reserve factor (RF) and on the minimum static aileron efficiency (C_{min}). These are described more in depth Sec. 4.2.

3.2 Continuous and Discrete Optimization phases

The full two-phases optimization process is presented in Figure 5. The first phase (Sec. 3.2.1) present the continuous optimization where the optimal LPs are obtained through a gradient-based process performed via MSC.Nastran SOL 200. Once the optimal LPs have been found, the corresponding stacking sequence is identified by mean of an inverse optimization problem via genetic algorithm (Sec. 3.2.2).

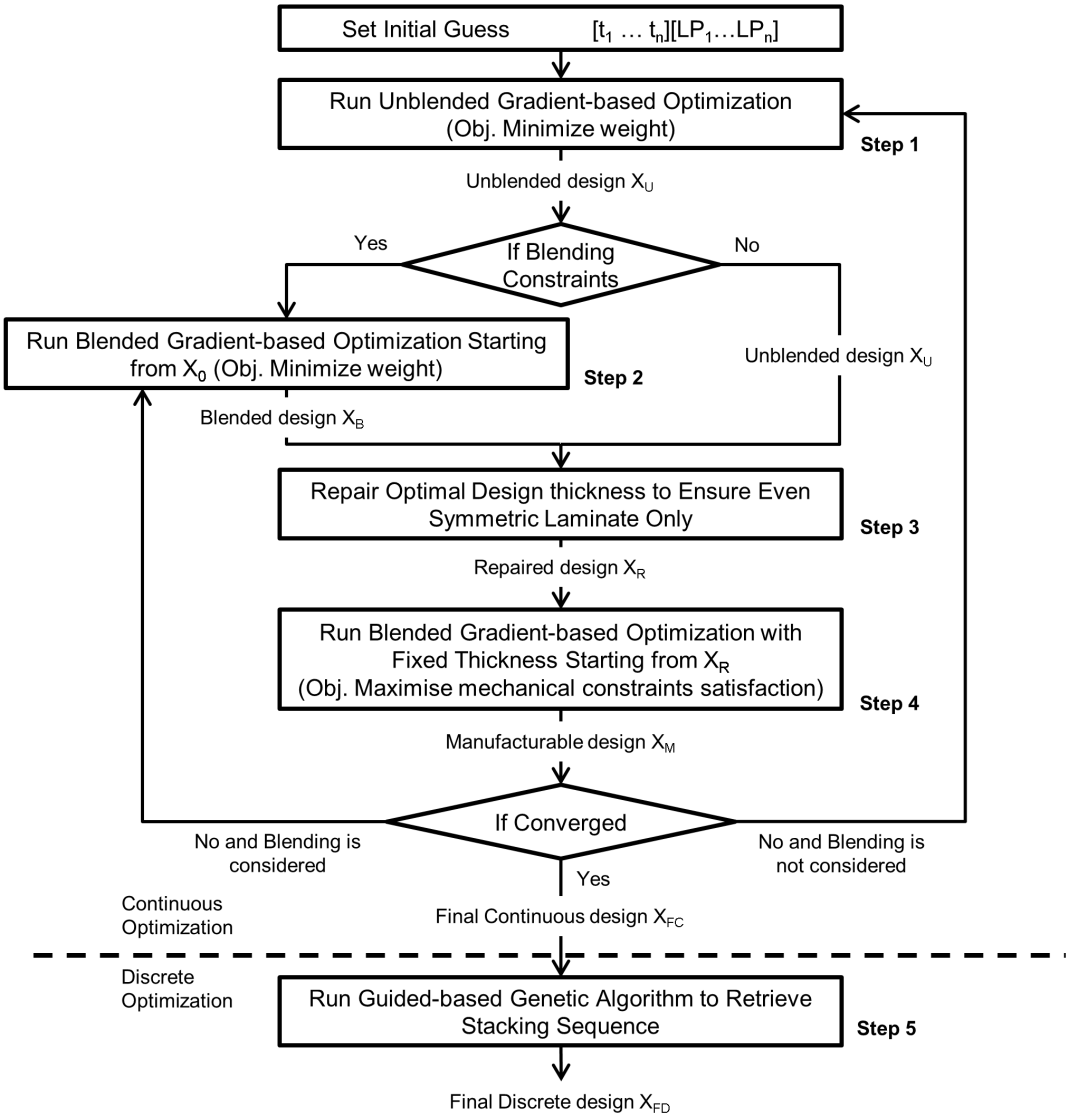

Figure 5: Proposed optimization strategy including blending constraints.

3.2.1 Continuous optimization

The blending constraints limit the change of lamination parameters between each section as function of their change in thickness. Applying those constraints while simultaneously optimizing thickness and lamination parameters leads to a non-convex optimization problem. Therefore, a 4-step strategy is employed in phase one or the optimization strategy (Figure 5).

For the case where blending constraints are enforced. The first step of this algorithm is the conventional convex optimization of the structure thicknesses and lamination parameters without blending constraints. This step provides a feasible starting point before the introduction of the blending con-

straints. The unblended design (X_U) is used as starting point for step 2, where blending constraints are considered. In step 3, a repair function rounds up the thicknesses of blended design (X_B) to an even number of plies. After the repaired design (X_R), lamination parameters are optimized one last time in step 4 while thicknesses are fixed. During this step, the feasibility of the structure is maximized, meaning that the objective function during this step is to maximize the reserve factors of all the mechanical constraints. Rounding of thicknesses and maximizing of reserve factors modify the stiffness of the structure, leading to internal load redistribution. Therefore, step 2-4 are repeated until convergence to a final continuous design (X_{FC}). After the final continuous design is obtained, a stacking sequence retrieval GA is employed to retrieve a blended final discrete design (X_{FD}). In case blending is not required, step 2 is avoided and steps 1,3-4 are repeated until convergence. The overall strategy is presented in Figure 5.

The optimizer and FEM solver used in this optimization is MSC.Nastran SOL 200, whereas the proposed strategy is implemented and run externally via Matlab script. The doublet lattice method (DLM) used to compute aeroelastic loads inside the static aeroelastic solver SOL144 have been corrected with rigid CFD computation to consider for wing profile camber and twist law (see Sec. 4.4).

3.2.2 Discrete optimization - Stacking sequence retrieval

The OptiBLESS [19] open source stacking sequence optimization toolbox is used to retrieve manufacturable laminates [1]. OptiBLESS uses a guide-based GA in order to retrieve blended stacking sequences matching the optimized lamination parameters achieved by the gradient-based optimizer (i.e. MSC.Nastran). According to the guide-based methodology [11], the thickest laminate is defined as the guide-laminate. Other laminates from the same structure are obtained by dropping plies from the guide-laminate therefore ensuring the final design is blended.

The outcome of the continuous optimization step is used as starting point for the discrete optimization. After the continuous optimization each wing section is optimized in terms of laminate thickness and lamination parameters. The thickest laminate within each substructure (i.e. skins and spars) is identified and set as the guide. Next, the ply angles describing the guide laminate stacking sequence and ply drops are used as design variables in OptiBLESS. Doing so ensure some level of structural continuity between each of the substructure laminates. That is, the plies of thinnest top skin laminate are ensured to span the entire top skin structure due to the guide-based coding implemented in OptiBLESS.

The genotype used in OptiBLESS to describe composite structures is given as:

$$Genotype = \left[\underbrace{[\theta_1\ \theta_2\ ...\ \theta_n]}_{\text{Ply angles}} \underbrace{[\Xi_1\ \Xi_2\ ...\ \Xi_D]}_{\text{Drop off}} \right] \tag{9}$$

The guide laminate is fully defined by the θ's. Other laminates are obtained by dropping plies from the guide stacking sequence. Since the number of plies associated with each section of structure is known from the continuous optimization, the ply drop off design variables denote which ply of guide stacking sequence must be dropped.

[1] `https://github.com/TMacquart/OptiBLESS`

The objective function used during the discrete optimization represents the lamination parameter matching quality between the continuous and discrete design. In other words, OptiBLESS is set to retrieve blended stacking sequences with lamination parameters matching the lamination parameters obtained at the end of the continuous optimization. This objective function is simply expressed as the root mean square error (RMSE) between the continuous and discrete lamination parameters as shown in Eqs. (10 and 11).

$$Fitness(\boldsymbol{\theta},\Xi) = \frac{1}{N_{lam}} \sum_{s=1}^{N_{lam}} RMSE_s(\boldsymbol{\theta},\Xi) \tag{10}$$

$$RMSE_s(\boldsymbol{\theta},\Xi) = \sqrt{\frac{1}{8}\sum_{i=1}^{8} w_i \left(\widetilde{\mathbf{LP}}_{i,s} - \mathbf{LP}_{i,s}(\boldsymbol{\theta},\Xi)\right)^2} \tag{11}$$

where N_{lam} is the total number of laminate sections in a structural component (i.e. upper wing skin), $\widetilde{\mathbf{LP}}_{i,s}$ is the vector of input parameters for section s, w_i is a weighting factor and $\mathbf{LP}_{i,s}$ is the vector of lamination parameters obtained by the GA. Stacking sequences are converted into lamination parameters in order to evaluate the fitness using the following notation:

$$\mathbf{LP} = [V_1^A\ V_2^A\ V_3^A\ V_4^A,\ V_1^D\ V_2^D\ V_3^D\ V_4^D] \tag{12}$$

According to the fitness function given in Eq. (10), the best retrieved stacking sequence would be a manufacturable stacking sequence exactly matching the optimized lamination parameters obtained by MSC.Nastran.

4 Model Description

4.1 Structural Model Description

The shell FE shell model is characterized by upper and lower skins, front and rear spars, 32 ribs, 13 stringers and represents a realistic aircraft regional aircraft wing. The structure is divided in sections each of them locally optimized by means its thickness and composite material anisotropy. In total there are 44 section, 14 for each skins and 8 for each spars Figure 6). Ribs and stiffeners do not take part in the optimization and are made of quasi-isotropic composite. Wing dimensions are presented in Table 1.

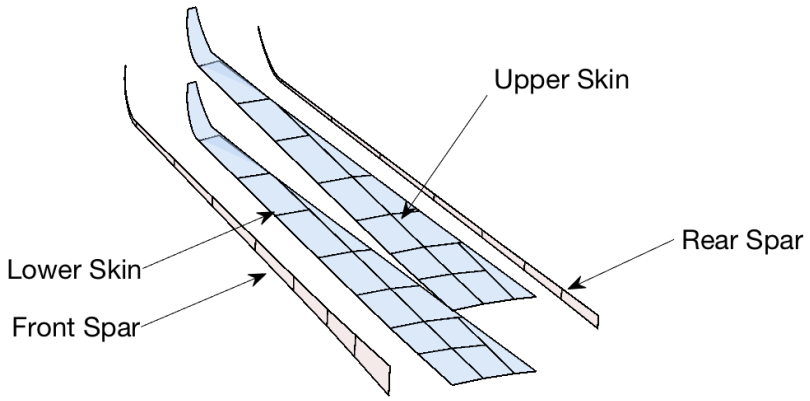

Figure 6: Wing used in the optimization divided in different section for local optimization.

Wing geometric characteristics	Values
Half Wingspan	16.7 m
Wing Area	111 m^2
Wing Dihedral	3.5°
Leading edge Sweep Angle	18°
MTOW	60,000 kg
Design cruise Mach	0.75

Table 1: Wing features.

4.2 Constraints

Two sets of structural constraints are active on the model. One set of constraints is represented by the material compatibility equations [20], these constraints ensure that each set of in-plane and out-of-plane lamination parameters leads to a realistic A and D stiffness matrix. The second set of constraints ensure that the model satisfies mechanical requirements such as strength and local buckling

The strength constraint used have been derive by IJsselmuiden et al. [21] and represent an analytical expressions for a conservative failure envelope based on the Tsai-Wu failure criterion in strain space. Local buckling is constrained via the closed formula Eq. (13) in all regions delimited by two ribs and two stiffeners and is enforced only in the wing skins.

$$\lambda_B = \pi^2 \frac{D_{11}(m/a)^4 + 2(D_{12} + 2D_{33})(m/a)^2(n/b)^2 + D_{22}(n/b)^4}{(m/a)^2 N_X + (n/b)^2 N_Y} \tag{13}$$

where buckling occurs for $\lambda_B < 1$, N_X and N_Y are the stresses in the longitudinal and transverse directions, a and b are the corresponding region dimensions and m and n are the corresponding number of half waves. A safety margin of 50% is applied to both strength and local buckling criteria.

A constrain on minimum aileron effectiveness is also imposed. It is formulated as follow:

$$C_{\min} = \frac{M_{\text{elastic}}}{M_{\text{rigid}}} \tag{14}$$

where M_{rigid} is the root bending moment created by deflecting the aileron on the rigid model, and M_{elastic} on the flexible model. $C_{\min}$ is constrained such as its value does not go bellow 10^{-4} at 1.2 times the speed reaching the maximum dynamic pressure.

4.3 Load cases

Different load cases are used in the optimization process. Table 2 summarized the maneuver loads:

N	Name	Mach	Altitude (ft)	Load factor (g)
1	Pull up	0.48	0	2.5
2	Push down	0.48	0	-1
3	Reversal	0.605	0	1

Table 2: List of the steady load cases used in the optimization.

As described in figure 4, the incremental gust loads are added to 1g flight loads, also computed at Mach 0.48. The different gust cases, taken from the certification CS25, are summarized Table 3:

N	Frequency (Hz)	Gust angle(deg)
1	9.06	2.97
2	7.40	3.075
3	5.73	3.21
4	4.07	3.395
5	2.40	3.71
6	0.74	4.51

Table 3: List of gust cases.

Using the aileron, maneuver load alleviation (MLA) can be performed during pull-up and push-down maneuver. The deflection setting is proportional to the load factor, therefore for the pull-up at +2.5G the deflection amplitude is two and a half times larger than for the push-down at -1G. The aileron is deflected upward during pull-up and downward during push-down. Finally, it is important to note that aerodynamic non-linearities such as flow separation around the aileron hinge are not implemented.

4.4 DLM correction

The aeroelastic loads are calculated via the MSC.Nastran static aeroelastic solver the utilize doublet lattice method (DLM). Since the aeroelastic loads coming from the DLM are use perform trim of the wing and calculate its displacement, it is important to correctly represent the spanwise and chordwise load distribution along the wing. This is achieved by using the concept of separation between the rigid and elastic load components, where the rigid part utilize rigid CFD results while the elastic increment is computed via DLM. This method, ofter referred to as hybrid static approach [22], allows to consider in the aeroelastic load computation for airfoil camber and wing twist law. This, not only ensures a more realistic lift distribution for structural sizing, but also provide correct wing deflection to the surrogate model so that the flexible load increment effect on on aerodynamic performance will be realistic, improving the fidelity of aircraft performance evaluation.

5 Results and Comments

5.1 Continuous step

In this section, results from various continuous optimizations are discussed. All optimizations performed in this section have been done using the approach showed in Sec. 4 where each of the loads were included when needed.

Optimization runs are executed with and without MLA in the two cases presented bellow. For the case with MLA, the aileron is deflected at 25° during pull-up and at $-10°$ for the push-down. Figures 7 and 8 show respectively, the highest failure indices for the two mechanical constraints (e.g. strength and local buckling) including all load cases shown in Tables 2 and 3 and the load cases associated to those high failure indices. One can observe that maneuvers are the main sizing cases for the wing box. Gust cases becomes critical when MLA is performed, reducing the relative importance of pull-up and

push down. It can also be noticed that for both set of results, the buckling is the most critical failure type. Therefore, the shift from having only the maneuvers sizing the wing box, toward a more complex mix of sizing load cases doesn't really affect the type of failure.

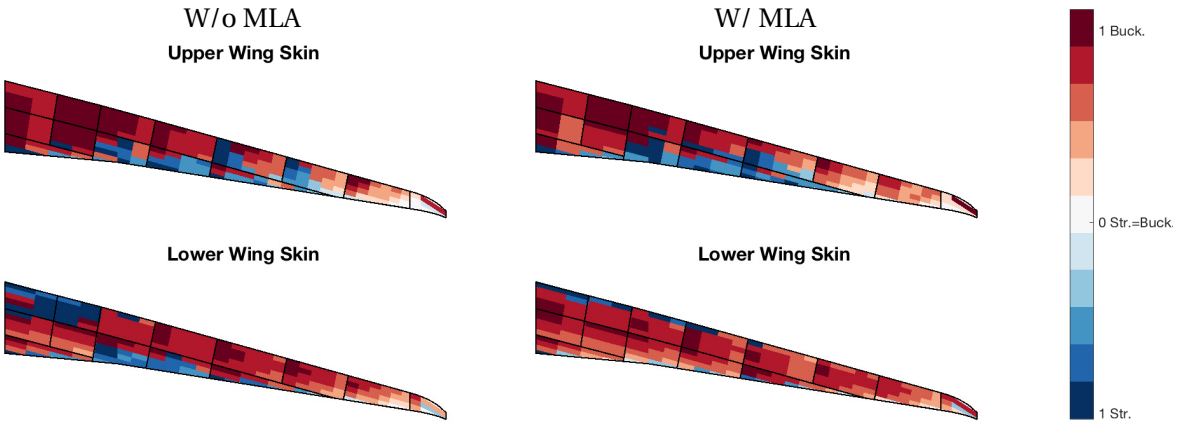

Figure 7: Highest failure indices, for the two mechanical constraints, among all load cases.

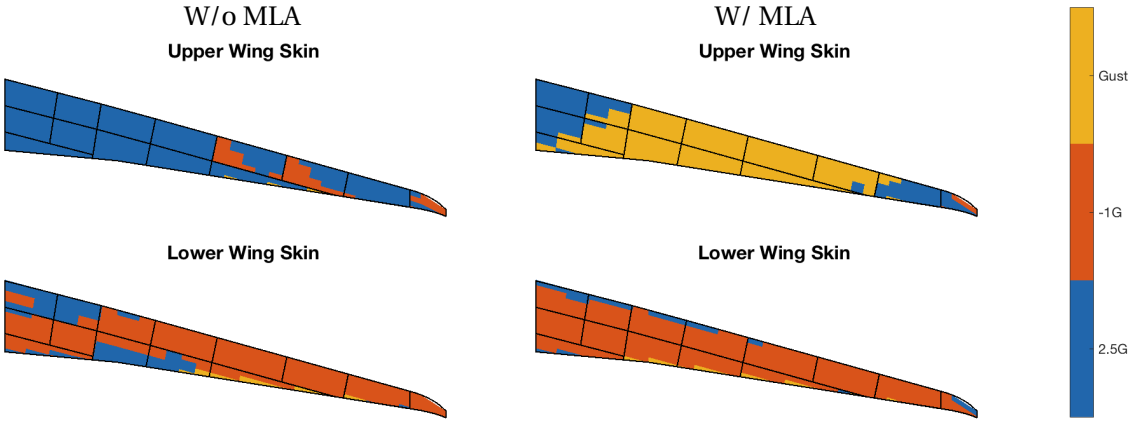

Figure 8: Load cases resulting in the highest failure indices for the two mechanical constraints.

A post-optimality study is then performed to assess wether the equivalent static load method (ESL) is able to fully constrain the mechanical responses at all time during a gust encounter. The study was performed on the case with MLA, where gust cases have some impact on the sizing. Shown on Figure 9 is the time history of the maximum value for both strength and local buckling during different load cases. Because they are the most critical ones, only the positive gust #4-5-6 listed on Table 3 are shown. This chart shows the effectiveness of the ESL method to constrain responses under dynamic loads, but also indicates that longer gusts of larger amplitude are the most important for sizing.

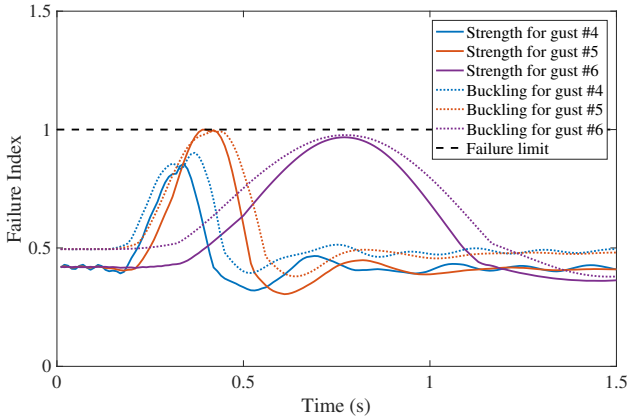

Figure 9: Maximum value of strength and buckling constraints during gusts #4-5-6 as function of time.

While aileron deflection can relief some root bending moment, it can also induce additional torsional loads, due to the aileron location at the rear of the wing. The best way to solve this trade-off is to resize the wing box and re-evaluate the weight for different aileron deflection values. The results of the study are plotted in Figure 10. The deflection angle on the x-axis is shown for the pull-up maneuver, its amplitude is two and a half smaller during push-down. One can observe that in case of a purely continuous optimization (no thickness round-up and no blending constraints) the wing weight will decreases as the aileron deflection increases. This isn't true anymore if blending constraints are used, inducing a minimum weight for 35° deflection. This could be explained as a result of the wing not being fully tailored for the more complex load path induced by a high aileron deflection. It can be observed that prior to the optimal deflection, the weight penalty induced by the blending constraints is relatively constant. As previously shown, the gust loads have little impact on the optimization when MLA is not used (aileron deflection at 0°). This behavior is here confirmed by noticing that the optimized weight with gust loads starts deviating around 20° of aileron deflection. The chart also show that the design space might not be fully convex, as small irregularities in the results from 0° to 15° are observed. It could explain why the design including gusts are lighter than the one without them for 10° and 15° of aileron deflection.

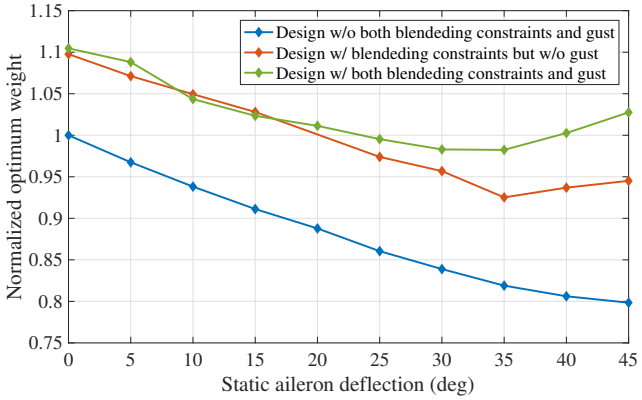

Figure 10: Optimum weight for various aileron deflection angle, with and without blending.

5.2 Discrete step

Among the tests performed is Sec. 5.1 the test case with static loads plus gusts have been used here to show the effectiveness of the blending constraints and the optimization strategy proposed in Sec. 3.2. Two different optimizations have been run, one without and one with the blending constraints with a shrinking factor α set to 0.5.

The difference in weight of the optimized solutions is shown in Figure 12 and lead to an increase of weight of about 4.65%. This weight increment is coherent with the reduction of the design space due to the inclusion of additional constraints. In Figure 11 the averaged RMSE obtain from 10 different stacking sequence retrieval is shown for the different problems. Results show that, even if not perfect match has been found in neither cases, stacking sequences closely matching the continuous optimum can be obtained thanks to the use of the blending constraints.

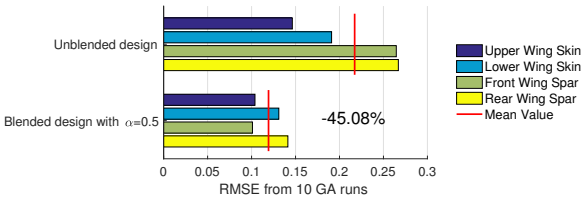

Figure 11: RMSE in stacking sequence retrieval via GA averaged over 10 runs.

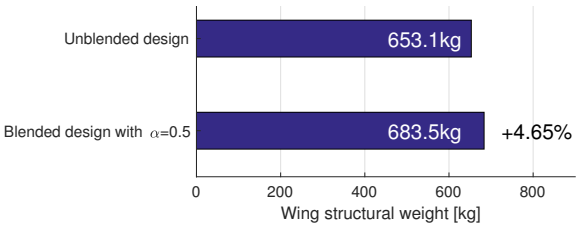

Figure 12: Weight of the optimized wing structure under static and gust loads.

Figures 14 and 14 present the thickness distribution for the two solutions. The solutions obtained with the blending constraints increases thickness uniformly along the full wing. This change in thickness is reflecting a change in stiffness orientation (see Figures 15 and 16). The stiffness orientation [6] represent the value of the in-plane stiffness component A_{11} in the panel and therefore allows for a visual representation of the main fiber direction. In the blended solution, thicknesses and stiffness directions in each panes are interconnected by means of the blending constraints. Therefore, the optimized is balancing the stiffness coming from thickness and from anisotropy in order to satisfy the blending requirements.

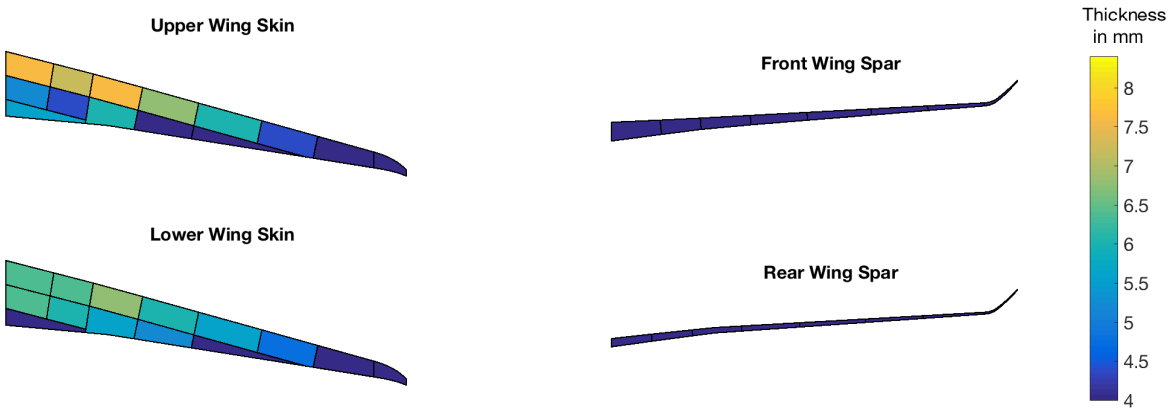

Figure 13: Thickness distribution along the wing for the unblended design.

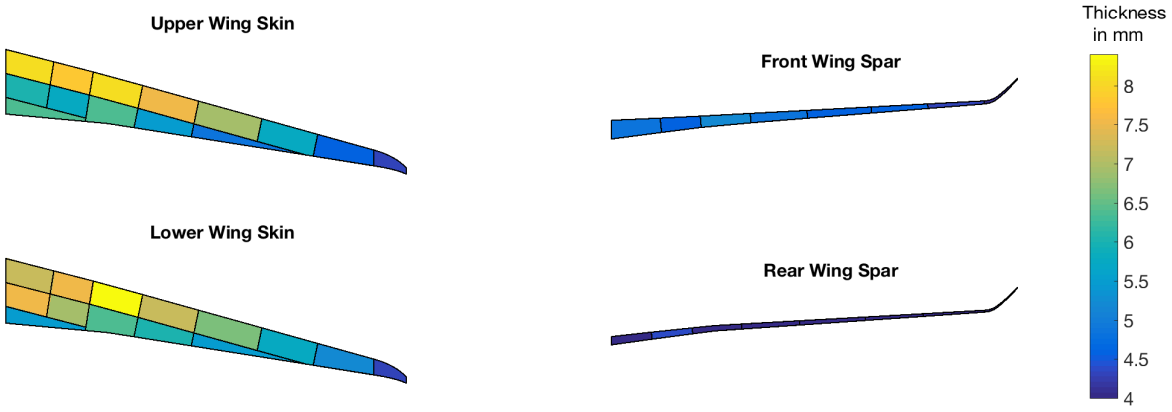

Figure 14: Thickness distribution along the wing for the blended design.

Spanwise and chordwise stiffness variation between the blended and unblended design is shows how the use of blending constraints helps in reducing stiffness local variation and results in a smooth variation between wing root and wing tip. This latter effect is clearly visible by comparing the lower skin and the front spar results shown in Figures 15 and 16.

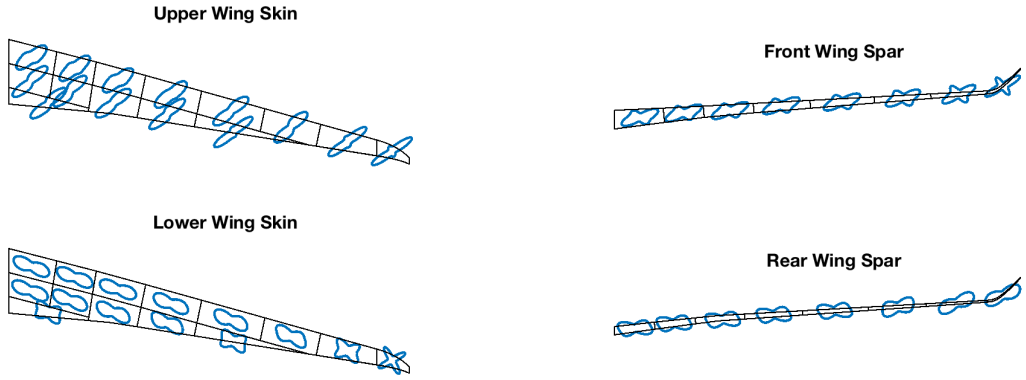

Figure 15: Stiffness distribution along the wing for the unblended design.

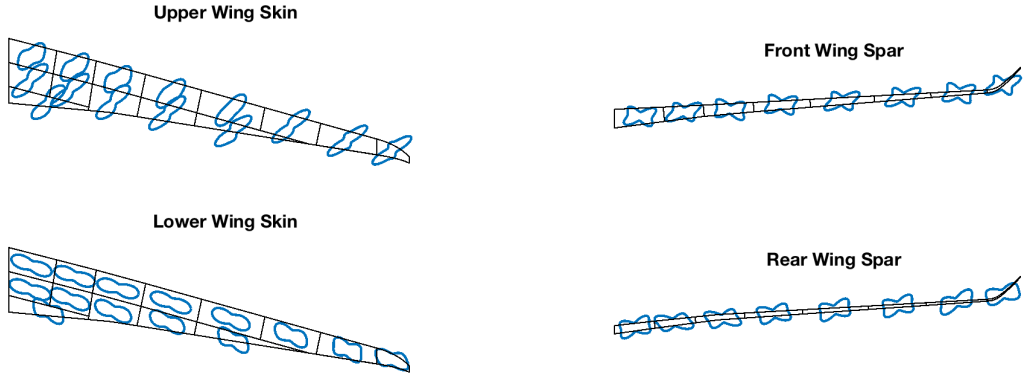

Figure 16: Stiffness distribution along the wing for the blended design.

However, even if blending constraints helped the optimized to find a continuous solution that could be more closely match by a discrete stacking sequence, the RMSE is still non zero (Figure 11). This means that while all constraints have been satisfied during the continuous optimization (see Figure 17), the now retrieved discrete stacking sequences are not guarantied to fulfill all mechanical constraints. Figures 17 and 18 show the valued of the mechanical constraints (i.e. strength and local bukling) at the end of the continuous optimization step and after the stacking sequence retrieval. Clearly enough not obtaining a 100% match between continuous and discrete designs leads to mechanical constraints violation with or without blending constraints. However, the use of the blending constraints greatly reduce the number for failed constraints and the magnitude of the failure indices (Table 4). The location of the highest failure indices presented in Figure 18 is shown in Appendix A.

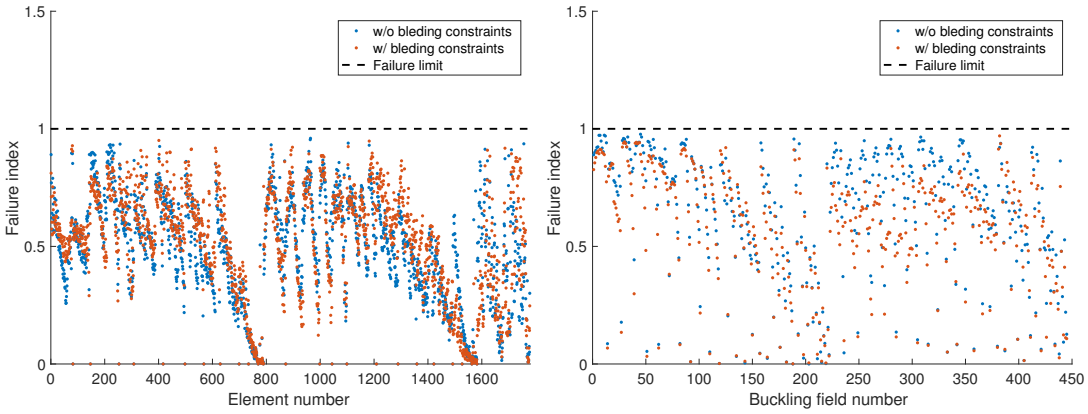

Figure 17: Strength and buckling constraints at the end of the continuous optimization. Failure occurs when FI>1.

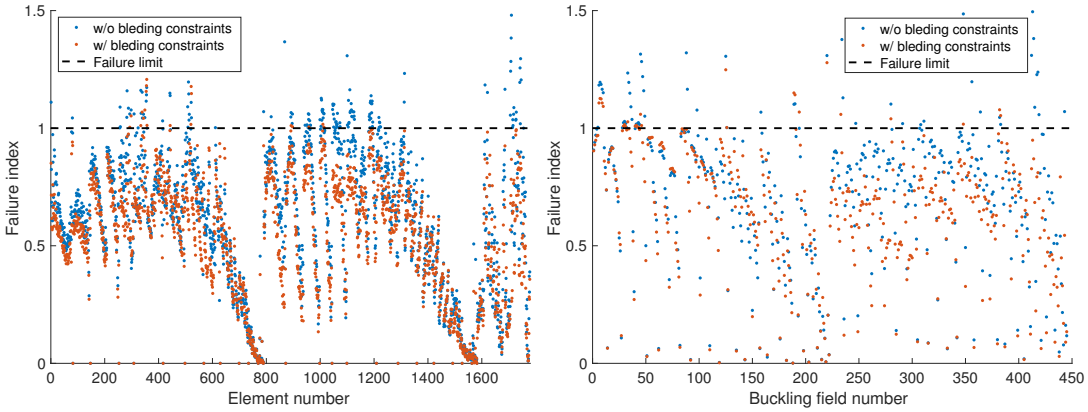

Figure 18: Strength and buckling constraints after stacking sequence retrieval. Failure occurs when FI>1.

	Failed Elements			**Max Failure Index**		
Mechanical constraint	No Blending	With Blending	Gain[%]	No Blending	With Blending	Gain[%]
Strength	142	19	86.6	1.4804	1.2073	18.8
Local Bucking	56	26	53.6	1.6160	1.2786	20.9

Table 4: Improvements in constraints violation after stacking sequence retrieval due to the use of blending constraints.

6 Conclusions and further works

The present paper investigates the effect of different load configurations in order to identify region of influence for different loads. The loads considered in the current work are static loads, gust loads and static loads with maneuver load alleviation (MLA). Gust loads have been included in the aeroelastic optimization via an equivalent static load (ESL). The different loads are applied to a regional aircraft composite wing that is optimized with respect to local panel thickness and composite anisotropy. Composite blending is tackled by means of continuous constraints and a two phases approach is proposed to find a blended stacking sequence table.

Results show that region of influence can be identified for specific loads. For the test case considered in this work, maneuvers load alleviation (MLA) is applied to the 2.5g and -1g load cases (without gust) showing its potential capabilities in reducing structural weight up to 20%. A smaller weight reduction is obtained when blending is taken into account. The inclusion of gust loads in the structural optimization result in various weight increment depending on the MLA setting. These confirm the importance of considering gust loads during preliminary design for aircraft incorporating MLA able to achieve a significant load reduction during maneuvers.

Finally, the composite wing structure under static and gust loads has been optimized with and without the blending constraints. The use of the blending constraints reduced by approximatively 45% the RMSE of the generic algorithm used to retrieved a blended stacking sequence. However this came at the price of a heavier design (+4.65%) due to the reduce design space. The reduced RMSE coming from the use of the blending constraints resulted in significant reduction of failed element and failure indices in the retrieved stacking sequence.

Further works will include multiple mass configurations for gust computations as well as different flight conditions, non-linear aerodynamics effect on aileron deflection for MLA and improvements in the stacking sequence retrieval performed via generic algorithm.

References

[1] Shirk, M. H., Hertz, T. J., and Weisshaar, T. A. (1986). Aeroelastic tailoring - theory, practice, and promise. *Journal of Aircraft*, 23(1), 6–18. doi:http://dx.doi.org/10.2514/3.45260.

[2] Jutte, C. and Stanford, B. K. (2014). Aeroelastic Tailoring of Transport Aircraft Wings: State-of-the-Art and Potential Enabling Technologies. Tech. rep.

[3] Grihon, S., Krog, L., and Bassir, D. (2009). Numerical Optimization applied to structure sizing at AIRBUS: A multi-step process. *International Journal for Simulation and Multidisciplinary Design Optimization*, 3(4), 432–442. ISSN 1779-627X, 1779-6288. doi:10.1051/ijsmdo/2009020.

[4] Kenway, G., Kennedy, G., and Martins, J. R. R. A. (2014). Aerostructural optimization of the Common Research Model configuration. In *15th AIAA/ISSMO Multidisciplinary Analysis and Optimization Conference*.

[5] Reimer, L., Ritter, M., Heinrich, R., et al. (2015). CFD-based Gust Load Analysis for a Free-flying Flexible Passenger Aircraft in Comparison to a DLM-based Approach. In *22nd AIAA Computational Fluid Dynamics Conference*.

[6] Dillinger, J. K. S. (2014). *Static Aeroelastic Optimization of Compisite Wing with Variable Stiffness Laminates*. Ph.D. thesis, Delft University of Technology.

[7] IJsselmuiden, S. T., Abdalla, M. M., Seresta, O., et al. (2009). Multi-step blended stacking sequence design of panel assemblies with buckling constraints. *Composites Part B: Engineering*, 40(4), 329 – 336. ISSN 1359-8368. doi:http://dx.doi.org/10.1016/j.compositesb.2008.12.002.

[8] Liu, B. (2001). *Two-Level Optimization of Composite Wing Structure Based on Panel Genetic Optimization*. Ph.D. thesis, Univeristy of Flodida.

[9] Macquart, T., Bordogna, M. T., Lancelot, P., et al. (2016). Derivation and application of blending constraints in lamination parameter space for composite optimisation. *Composite Structures*, 135, 224 – 235. ISSN 0263-8223. doi:http://dx.doi.org/10.1016/j.compstruct.2015.09.016.

[10] Bordogna, M. T., Macquart, T., Bettebghor, D., et al. (2016). Aeroelastic optimization of variable stiffness composite wing with blending constraints. 17th AIAA/ISSMO Multidisciplinary Analysis and Optimization Conference. doi:10.2514/6.2016-4122.

[11] Adams, D. B., Watson, L. T., Gurdal, Z., et al. (2004). Genetic algorithm optimization and blending of composite laminates by locally reducing laminate thickness. *Advances in Engineering Software*, 35(1):35-43.

[12] Campen, J. V., Seresta, O., Abdalla, M. M., et al. (2008). General blending definitions for stacking sequence design of composite laminate structure. 49th AIAA/ASME/ASCE/AHS/ASC structures, structural dynamics, and materials, pp. 7–10.

[13] Tsai, S. W. and Hahn, H. T. (1980). *Introduction to composite materials*. Technomic Publishing Co.

[14] Grenestedt, J. and Gudmundson, P. (1993). Layup optimization of composite material structures. In P. PEDERSEN (Ed.), *Optimal Design with Advanced Materials*. Oxford: Elsevier. ISBN 978-0-444-89869-2, pp. 311 – 336. doi:http://dx.doi.org/10.1016/B978-0-444-89869-2.50027-5.

[15] Kang, B. S., Park, G. J., and Arora, J. S. (2006). A review of optimization of structures subjected to transient loads. *Structural and Multidisciplinary Optimization*, 31(2), 81–95.

[16] Kang, B. S., Choi, W. S., and Park, G. J. (2001). Structural optimization under equivalent static loads transformed from dynamic loads based on displacement. *Structural and Multidisciplinary Optimization*, 79(2), 145–154.

[17] Bettebghor, D., Blondeau, C., Toal, D., et al. (2013). Bi-objective optimization of pylon-engine-nacelle assembly. *Structural and Multidisciplinary Optimization*, 48(3), 637–652.

[18] Park, G. J. (2006). Technical overview of the equivalent static loads method for non-linear static response structural optimization. *Structural and Multidisciplinary Optimization*, 43, 319–337.

[19] (2016). *Optibless - an open-source toolbox for the optimisation of blended stacking sequences (accepted). In The seventeenth European Conference on Composite Materials (ECCM17)*.

[20] Raju, G., Wu, Z., and Weaver, P. (2014). On further developments of feasible region of lamination parameters for symmetric composite laminates. In *55th AIAA/ASME/ASCE/AHS/ASC Structures, Structural Dynamics, and Materials Conference, AIAA SciTech, (AIAA 2014-1374)*. doi:http://dx.doi.org/10.2514/6.2014-1374.

[21] Ijsselmuiden, S. T., Abdalla, M. M., and Gurdal, Z. (2008). Implementation of strength-based failure criteria in the lamination parameter design space. *AIAA Journal*, 46(7), 1826–1834.

[22] Vincenzo, F. G. D. (2012). Hybrid static aeroelasticity new capabilities - cfd data management.

Acknowledgement

Paul Lancelot is grateful for the founding by the European Community's CleanSky 2 Programme under Horizon 2020 (H2020) under the Grant Agreement 686804. The ReLOAD project (Regional turboprop Loads control through active and passive technologies) is a CfP project funded under the Regional IADP involving 2 partners. The project started on 1 December 2015.

Appendix A

Figure 18 shows the highest failure indices for the two mechanical constraints (e.g. strength and buckling) among all load cases. In Figures 19, 20, 21 and 22 the location of such failure indices on the wing is shown.

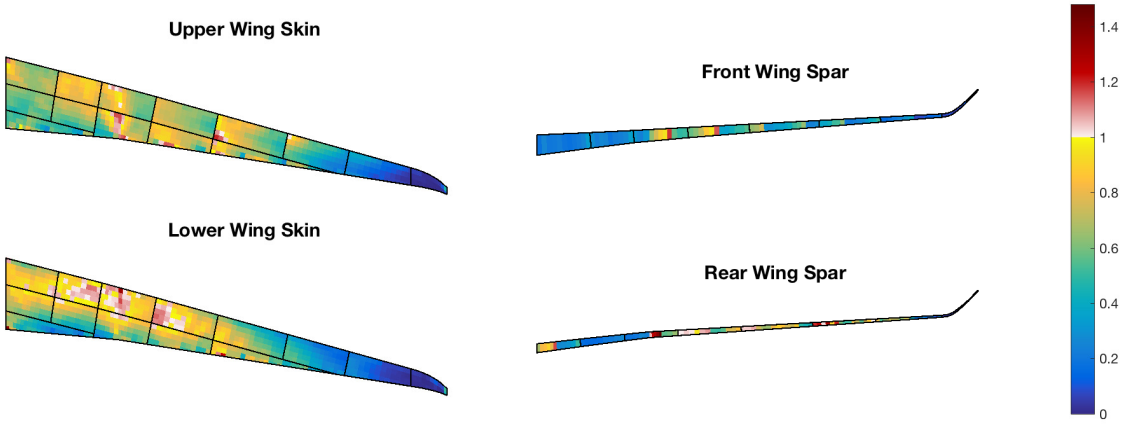

Figure 19: Location of the highest failure indices in strength after stacking sequence retrieval from continuous optimum obtained without blending constraints.

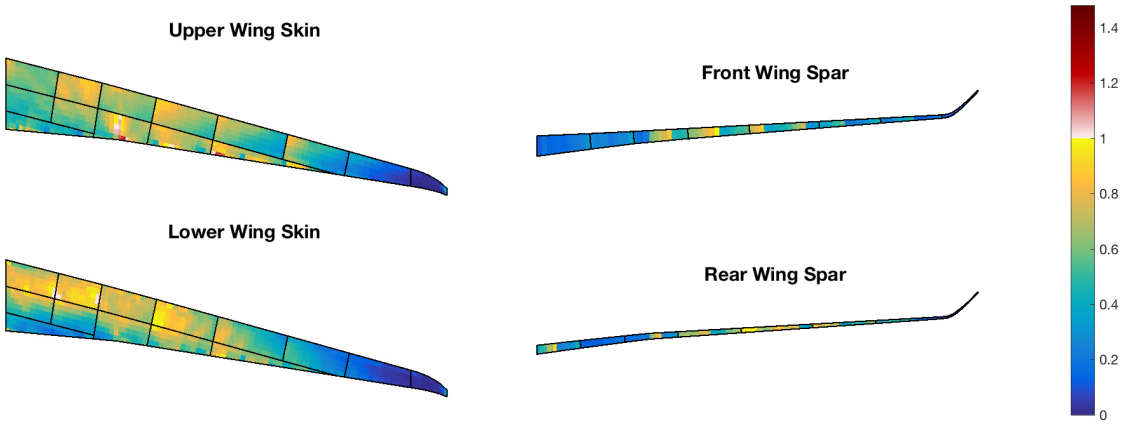

Figure 20: Location of the highest failure indices in strength after stacking sequence retrieval from continuous optimum obtained with blending constraints.

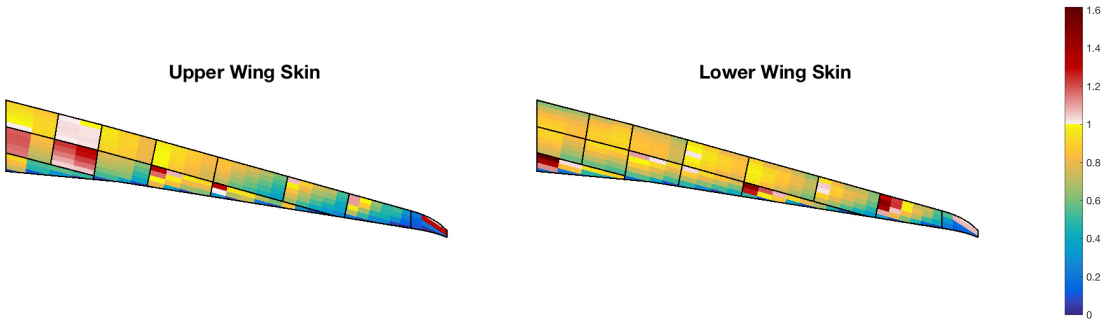

Figure 21: Location of the highest failure indices in local buckling after stacking sequence retrieval from continuous optimum obtained without blending constraints.

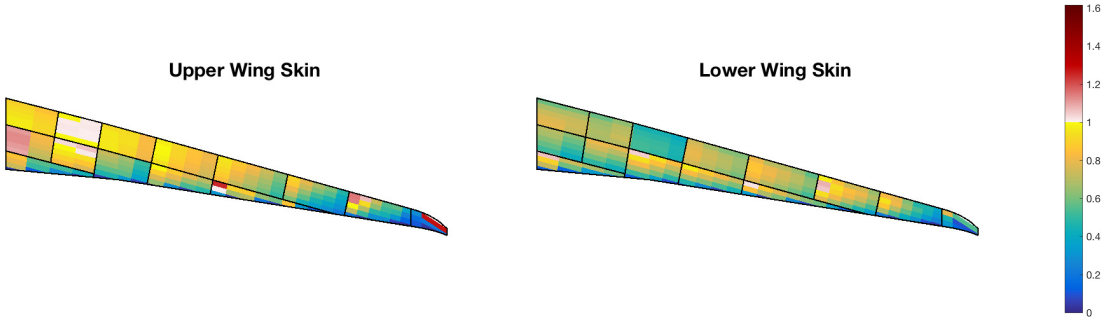

Figure 22: Location of the highest failure indices in local buckling after stacking sequence retrieval from continuous optimum obtained with blending constraints.